Metallocatanionic vesicles mediated enhanced singlet oxygen generation and photodynamic therapy of cancer cells

Bunty Sharma[1,2,a], Akhil Jain[3,a], Lluïsa Pérez-García[2,4,5*], Julie A Watts[3], Frankie J. Rawson[3], Ganga Ram Chaudhary[1], and Gurpreet Kaur[1*]

[1] Department of Chemistry, Centre for Advanced Studies in Chemistry, Panjab University, Chandigarh-160014, India

[2] Division of Advanced Materials and Healthcare Technologies, School of Pharmacy, University of Nottingham, Nottingham NG7 2RD, UK

[3] Division of Regenerative Medicine and Cellular Therapies, School of Pharmacy, University of Nottingham, Nottingham NG7 2RD, UK

[4] Departament de Farmacologia, Toxicologia i Química Terapèutica, Facultat de Farmàcia i Ciències de l'Alimentació, Avda. Joan XXIII 27-31, Universitat de Barcelona, 08028 Barcelona, Spain

[5] Institut de Nanociència i Nanotecnologia UB (IN2UB), Universitat de Barcelona 08028 Barcelona, Spain

[a]These authors have contributed equally to this work.

*corresponding authors: Gurpreet Kaur (email: gurpreet14@pu.ac.in)

Lluisa Perez-Garcia (email: mlperez@ub.edu)

Abstract: In clinics, photodynamic therapy (PDT) is established as a non-invasive therapeutic modality for certain types of cancers and skin diseases. However, due to poor water solubility, photobleaching and dark toxicity of photosensitizers (PSs), further developments are required to improve the efficiency of PDT. Herein, we report the role of metallocatanionic vesicles (MCVs) in enhancing the phototoxicity of methylene blue (MB) against cancer cells. These MCVs were prepared by a facile and quick solution-solution mixing method using a cationic single-chain metallosurfactant (FeCPC I) in combination with the anionic sodium oleate (Na Ol). For singlet oxygen ($^1O_2$) generation and PDT studies, two fractions FeCPC I:Na Ol (30:70) and (70:30) were chosen based on their long-term stability in aqueous media. A cationic PS MB was loaded into these vesicles. The MB-loaded MCVs 30:70 and 70:30 fractions enhanced the $^1O_2$ generation by 0.10 and 0.40 fold, respectively, compared to MB alone. Upon illumination with a 650 nm laser, these MB-loaded V73 (70:30) and V37(30:70) MCVs significantly decreased the metabolic activity of MCF-7 cells by ≤50% at a concentration of 0.75 µM. Furthermore, the SOSG assay revealed that the synthesized MCVs enhanced the intracellular $^1O_2$ compared to MB alone. MB-loaded V73 MCVs showed the highest $^1O_2$ mediated membrane damage and cell killing effect as confirmed by differential nuclear staining assay (DNS), which is attributed to the cellular uptake profile of different MCV fractions. Altogether this work shows the advantage of using these biocompatible and dual charge MCVs as promising delivery vehicles that can enhance the $^1O_2$ generation from PS. This work endows the future application of these Fe-MCVs in magnetically guided PDT.

Keywords: Metallosurfactants, catanionic vesicles, methylene blue, singlet oxygen, photodynamic therapy

1. Introduction:

Photodynamic therapy (PDT) is a non-invasive fourth modality treatment approved by the FDA for the treatment of a variety of cancers [1]. The principal advantage of PDT over traditional chemotherapy or radiotherapy is its non-invasive nature and negligible side effects as oxidative damage only occur in the proximity of the PS [2-4]. In general, PDT requires a combination of three non-chemotoxic essential components viz. photosensitizer (PS), the light of specific wavelength, and molecular oxygen ($^3O_2$). PDT relies on the generation of reactive oxygen species (ROS) from a photosensitizer upon activation by light of a specific wavelength, which eventually induces membrane damage and cell death [5,6]. ROS are generated either through charge transfer which generates radicals and superoxide (type I mechanism of PDT). In the type II mechanism, singlet oxygen ($^1O_2$) is generated due to the transfer of energy from the excited triplet state of the PS to $^3O_2$. Therefore, achieving high efficiency of $^1O_2$ generation from PS is one of the most important prerequisites for clinical application of PDT [7,8].

In recent years, a range of PSs such as PPIX, phthalocyanine, and verteporfin has been explored for PDT and a few of them have been approved by FDA for their use in clinics [1]. However, most of these PSs are hydrophobic with absorption maxima in UV which causes poor bioavailability and limited penetration depth that leads to diminished PDT efficiency in clinical settings [7,8]. On the other hand, Methylene Blue (MB) is a tricyclic phenothiazine cationic dye approved for the treatment of methemoglobinemia. Due to its photophysical properties such as broad absorption band (550-700 nm) with absorption maxima at 664 nm and excellent solubility in physiologically relevant media it has been extensively studied for PDT against different cancers and bacterial infection. However, under physiological conditions, MB forms aggregate to form dimers which significantly reduces its ability to generate $^1O_2$ thus impacting its therapeutic effectiveness [9,10]. Therefore, the design and

formulation of new biocompatible delivery vehicles that allow the encapsulation of MB at an adequate therapeutic level without affecting its chemical and photophysical properties are of great importance.

To date, many nanoscale delivery vehicles have been investigated and among them, vesicles have always been one of the preferred choices due to stable and have the ability for further improved chemical functionalization and physiological applications [11]. Mixing of cationic/anionic surfactant in a non-equimolar ratio leads to the spontaneous formation of a catanionic mixture which is known as catanionic vesicles (CVs) [12,13]. These catanionic vesicles have interesting physicochemical properties such as adjustable size, surface charge, and high permeability to skins by varying the cationic/anionic ratio and surfactant chain length [14-16]. Hybrid stimuli-responsive CVs can also be prepared by using pH, redox, and temperature-sensitive cationic and anionic surfactant for encapsulation of both hydrophilic/hydrophobic and cationic/anionic drugs for drug delivery applications [17]. On the other hand, metallosurfactants are hybrid surfactants that are prepared via the incorporation of metal into the molecular structure of surfactants [18]. Our group has previously reported different single and double-chain cationic metallosurfactant based nano-colloids for various applications for instance in catalysis, anti-corrosion, and drug delivery [19-22]. These metallosurfactant surfactants have gained considerable interest due to the dual inherent properties of metal and surfactant which self-assembled at low concentration as compared to parent surfactant. By using these metallosurfactant as cationic components a new hybrid metallocatanionic vesicles (MCVs) are synthesized, which carry dual metal and surfactant with both cationic and anionic surface charge.

Herein, we report the synthesis of MCVs from single-chain Iron-metal based surfactant i.e. hexadecyl pyridinium trichloro ferrate $[Cp]^{+}[FeCl_3]^{-}$ (FeCPC I) combined with anionic single-chain sodium oleate (Na-Ol) fatty acid. These synthesized vesicles were characterized

by dynamic light scattering (DLS), cryo-transmission electron microscope (cryo-TEM), and field emission gun scanning electron microscopy (FEG-SEM). These MCVs were then used for the delivery of cationic PS (MB) for photodynamic therapy of MCF-7 breast cancer cell lines. Furthermore, the capability of MB-loaded vesicles to generate $^1O_2$ in solution and intracellularly was evaluated using 9, 10-anthracenediyl-bis(methylene) dimalonic acid (ABMA) and singlet oxygen sensor green (SOSG), respectively. These MB-loaded FeCPC I: Na-Ol showed negligible toxicity under dark, while on the other hand, an enhanced $^1O_2$ generation and the cell-killing effect was observed upon irradiation with a deep red laser (650 nm) for 10 min. To the best of our knowledge, this is the first study that reports on the application of metallocatanionic vesicles for $^1O_2$ mediated photodynamic therapy against cancer cells.

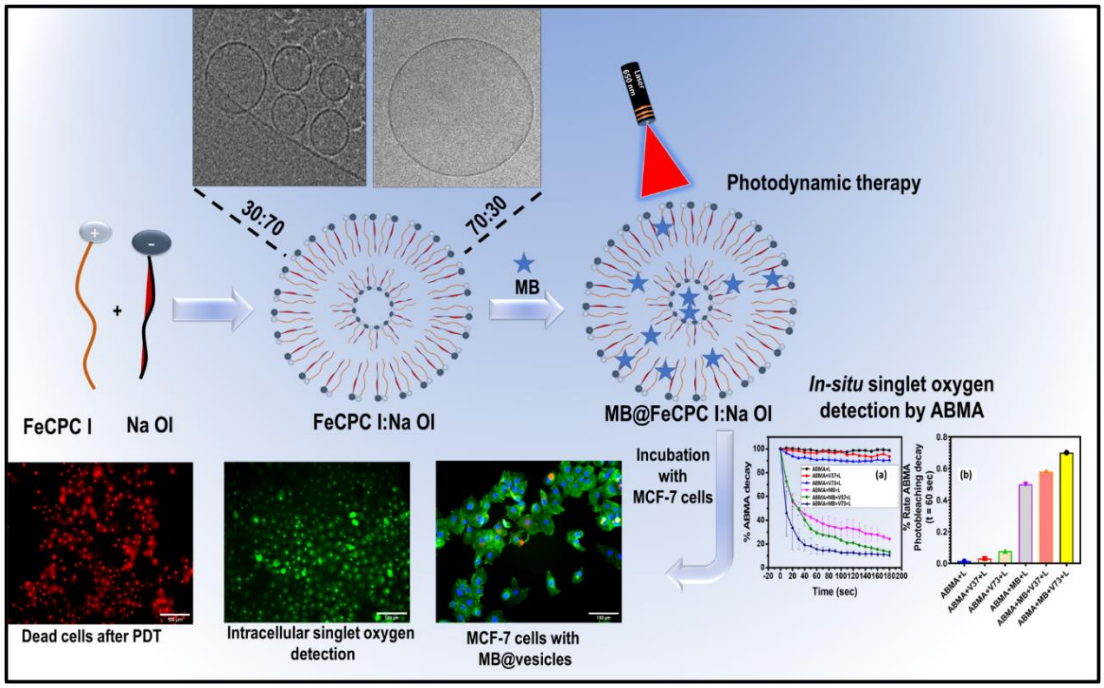

Scheme 1. Schematic representation of metallocatanionic vesicles formation from FeCPC I: Na-Ol and subsequent loading of MB and their uses in photodynamic therapy.

2. Experimental section

2.1. Materials

All the chemicals used were of analytical grade and were used as supplied without further purification and modifications unless specified. Sodium Oleate [$C_{18}H_{33}NaO_2$] Na Ol, Methylene Blue (MB), 9,10-Anthracenediyl-bis(methylene) dimalonic acid (ABMA), Cell Counting Kit-8 (WST-8) and Propidium Iodide (PI) were purchased from Sigma Aldrich (UK). Singlet Oxygen Sensor Green (SOSG) and Hoechst 33342 were purchased from Thermo Fischer Scientific, UK.

2.2. Methodology

2.2.1 Synthesis of metallocatanionic vesicles: Single-chain cationic iron metal-based metallosurfactant (hexadecylpyridinium iron (II) trichloride; FeCPC I) was prepared by following a protocol previously reported [23]. In brief, MCVs were synthesized using single-chain cationic metallosurfactant (FeCPC I) in combination with anionic single chain fatty acids Na Ol. A 1 mM solution of cationic and anionic surfactant was prepared separately in PBS. The solution was sonicated for 10 min and then mixed in different ratios of FeCPC I:Na Ol from 10:90 to 90:10. Finally, a gentle shaking for 10 min led to the formation of vesicular aggregates. In the manuscript, FeCPC I:Na Ol vesicle are represented as V19 or fraction (10:90) which consists of 10 % FeCPC I and 90% Na Ol and V91 or fraction (90:10) with 90% FeCPC I and 10% Na Ol.

2.2.2. Characterization of metallocatanionic vesicles: Different techniques were used to characterize the fabricated vesicles. The mean hydrodynamic diameter (in nm), Polydispersity index (PDI), and zeta potential (mV) was estimated using Zetasizer Nano ZS (Malvern Panalytical, UK). The stability of these vesicles in PBS (pH = 7.4) was studied for a period of 1 month by measuring the hydrodynamic diameter and PDI. The morphology of colloidal structural aggregates of vesicles was characterized by cryo-TEM, JEOL 2100 plus TEM operating at 200kV, with the sample held at or below –176°C: images recorded using a Gatan US1000XP with a nominal defocus of 3-5 µm. The sample was prepared by depositing

3 µL liquid onto a TEM grid (GO/C/300 mesh Cu) in a controlled environment (20°C, 78° humidity), blotting (1.5s) before plunging into liquid ethane to vitrify (Gatan CP3 cryo plunge). The sample was maintained under liquid nitrogen during storage and transfer to TEM using a Gatan 626 cryo holder and a Gatan (Smartest model 900) cold stage controller. The field emission gun scanning electron microscope (FEG-SEM) was utilized to study the surface morphology of the synthesized vesicles before and after loading the photosensitiser. A fresh sample of vesicles in PBS was casted on an aluminum stub and then dried overnight under vacuum. Later, the samples were coated with a 5 nm thick layer of iridium and finally imaged on JEOL 7100F operating at 5 kV. Fluorescence spectra of the MB-loaded MCVs were acquired using a FLS 980 spectrometer in a quartz cuvette. Next, Inductively coupled plasma mass spectroscopy (ICP-MS) (iCAPQ Thermo Fischer) study was performed to check the amount of Fe present in V73 and V37 fractions. Final MCVs fractions solution prepared 2% HNO_3 acidic solution.

2.2.3. MB encapsulation: The encapsulation efficiency (%) of MB was evaluated using a protocol reported earlier [24,25]. MB solution was mixed with MCVs: V37 and V73 fractions and sonicated for 15 min and then kept for shaking for another 3 h. Finally, MB containing MCVs fractions were centrifuged at 13000 rpm followed by filtering. Fluorescence spectroscopy was used to record the fluorescence spectra of pure MB and MB-loaded MCVs. The encapsulation efficiency was calculated using the following equation:

$$\text{Encapsulation efficiency (\%)} = (I_{max} - I_0)/I_{max} \times 100 \quad (1)$$

Where I_0 is the fluorescence intensity of MB after loading into MCVs fraction and I_{max} is the MB fluorescence intensity without MCVs.

Further, High resolution transmission electron microscope (HR-TEM) and FEG-SEM analysis were performed to check the MB@MCV V37 and V73 fractions morphology.

2.2.4. Detection of Singlet oxygen generation by ABMA assay: A chemical trapping method was used to evaluate the $^1O_2$ generation capability of MB-loaded MCVs. For quantification of $^1O_2$, ABMA a water-soluble $^1O_2$ trapping dye was used [26]. In brief, ABMA (2 uM) was mixed with either free MB or MB-loaded MCVs. The mixture was irradiated with a red diode laser (650 nm and 50 mW; purchased from ADLABS, India) for different periods of time. The efficiency of $^1O_2$ generation was determined by monitoring the decrease in fluorescence emission intensity of the ABMA at 405 nm. Quantification of the generation of $^1O_2$ as a function of percentage decay in ABMA fluorescence was calculated using the following equation:

$$\text{The maximum rate of ABMA photobleaching} = \frac{(\%\ \text{IF at t= 0 sec}) - (\%\ \text{IF at t=60 sec})}{60\ \text{sec}\ X\ \text{Methylene Blue}\ (\mu\text{M})} \qquad (2)$$

Where, IF is the fluorescence intensity of ABMA at 405 nm.

2.2.5. Cell culture- Human breast cancer cells MCF-7(ATCC, USA) were cultured in high glucose Dulbecco's Modified Eagle's Medium (DMEM) supplemented with 10% fetal bovine serum (FBS) from Gibco with 1% penicillin/streptomycin. Cells were maintained in a humidified incubator containing 5% CO_2 at 37 °C.

2.2.6. WST-8 metabolic activity assay - A cell counting kit (CCK-8) was used to evaluate the dark and phototoxicity of MB-loaded MCVs on MCF-7 cells. For dark toxicity, a total of 5×10^3 cells/well were seeded in a 96 well plate and incubated for 24 h. Afterward, culture media was replaced with fresh media containing either MB (0.5µM) or plain MCVs viz.V37 and V73 or MB loaded vesicles at different concentrations (0.05, 0.1, 0.2, 0.5, and 0.75 µM) and incubated for 24 h. The concentration of MB was fixed at 0.5 µM in all the MCVs. Later, the cells were washed twice with PBS and 100 µL fresh media was added and cells were further incubated for 24 h. Next, the media was replaced with a mixture of DMEM containing 10 % CCK-8. The cells were incubated for 3 h at 37 °C and 5% CO_2. Finally, the absorbance of the plate was read at 450 nm using a Tecan microplate reader. All the experiments were

performed in triplicate and were repeated twice. For phototoxicity studies, the media of cells (24 h after seeding) was replaced with fresh media containing MB (0.5 µM) or MB containing vesicles V37 and V73 or plain vesicles at a concentration of 0.2 and 0.75 µM followed by 24 h incubation. Afterward, cells were washed twice with PBS and fresh media was added. Next, the plate was irradiated with a red laser (650 nm; power = 50 mW) at different doses and incubated for 24 h before measuring absorbance at 450 nm. Absorbance reading of untreated cells in the culture medium was used for baseline correction.

2.2.7. Cellular uptake study- For cell uptake analysis, MCF-7 cells were seeded in a 96-well plate at a density of 5×10^3 cells/well and incubated for 24 h. Then, the culture media was replaced with fresh media containing either MB (2 µM) or MB-loaded vesicles (V37 and V73), and the plate was further incubated for another 24 h to facilitate the uptake of MCVs. Afterward, the cells were washed thrice with PBS to remove unbounded MB-loaded vesicles and incubated for another 24 h. Finally, the cells were fixed with 4% paraformaldehyde for 15 min followed by Actin phalloidin stain for 30 min. and DAPI for 20 min. Between each staining step the cells were washed thrice with PBS. Finally, the plate was imaged using a fluorescence microscope (Nikon eclipse Ti) at 20X objective. The nuclei, actin, and MB were imaged using DAPI, FITC, and mPlum filters, respectively.

***2.2.8. Invitro* singlet oxygen detection-** MCF-7 cells were seeded at a density of 5×10^3 cells/well in tissue culture-treated black glass-bottom 96-well plate and incubated for 24 h at 37 °C and 5% CO_2 atmosphere. Next, the media of the cells was replaced with media containing either free MB (0.5 µM) or MB-loaded MCVs viz V73 and V37 at a concentration of 0.2 and 0.75 µM. After 24 h of incubation, cells were washed twice with PBS and the media was replaced with SOSG (10 µM) in PBS solution and incubated for 20 min. Later, each well of the plate was irradiated with a 650 nm red diode laser for 10 min. Finally, the

cells were washed with PBS and the green fluorescence of SOSG was observed as a function of $^1O_2$ generation using a Nikon eclipse Ti with FITC filter settings.

2.2.9. DNS assay- Hoechst/Propidium Iodide (PI) differential nuclear staining was performed to detect the % of dead cells. The cells were seeded at a density of 5×10^3 cells/well in 96 well glass bottom black plates. After 24 h incubation, the media was replaced with MB-loaded vesicles at a concentration of 0.75 µM and further incubated for 24 h. After the incubation period, the plate was washed with PBS and fresh media was added followed by irradiation with 650 nm laser for 10 min followed by incubation for another 4 h. Afterward, the cells were washed gently with PBS, and PI solution was added (0.25 mg/mL in PBS) and incubated for 10 min at room temperature. Next, the cells were washed with PBS twice and 100 µL Hoechst was added to each well and left for 20 min at room temperature. Finally, the plate was imaged using a Nikon eclipse Ti fluorescent microscope with DAPI and mCherry filter settings.

3. Result and Discussion:

3.1. Preparation and characterization of MCVs:

The cationic metallosurfactant was synthesized using a protocol reported earlier [23]. In brief, a ligand insertion synthesis method was employed which contained a 1:1 ratio of iron metal in combination with cetylpyridinium chloride (CPC). A facile and quick solution-solution mixing method with high reproducibility was utilized for the synthesis of MCVs. An anionic single-chain fatty acid was employed for the synthesis of MCVs fractions by mixing cationic metallosurfactant and an anionic surfactant. These cationic and anionic parts were dissolved in PBS (pH = 7.4) and sonicated for 10 minutes to obtain a homogenous solution and then finally mixed in different ratios, which spontaneously led to the formation of vesicles. Fig. 1 (A) represents the cationic FeCPC I and anionic Na Ol component surfactant. Fig. 1(B)

shows FeCPC I:Na Ol (total 1 mM concentration) fractions from 1:9 to 9:1 ratio, labeled as V19 to V91. The anionic rich fractions were more turbid while cationic rich fractions were colored which is due to cationic FeCPC I. While Fig. 1(C) is for 0.1 mM concentration of FeCPC I:Na Ol fractions which appeared to be clear on both cationic and anionic sides.

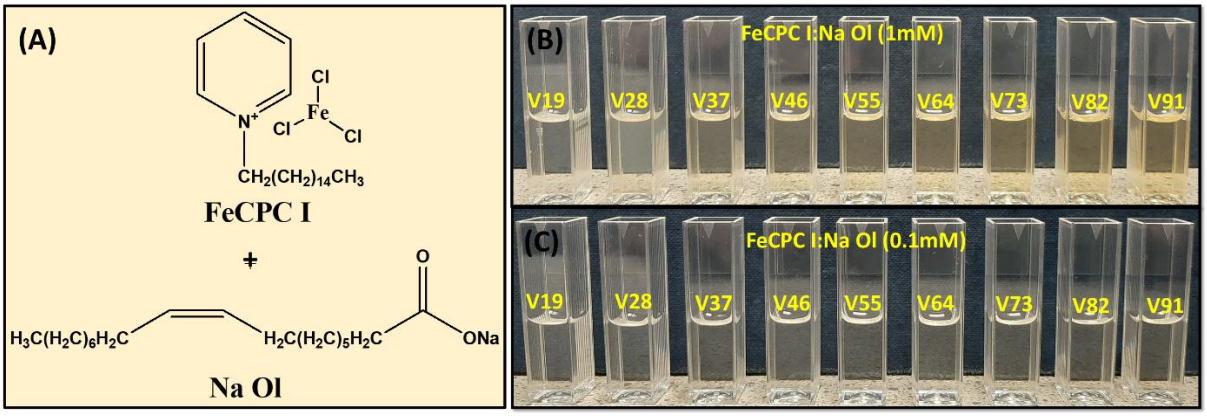

Fig. 1 Metallocatanionic vesicles component surfactant and prepared fractions (A) Structure of FeCPC I and Na Ol component surfactant. Images of the fractions prepared from FeCPC I:Na Ol **(B)** 1 mM and **(C)** 0.1 mM mixing in PBS solution. Where V19 and V91 indicate 10:90 and 90:10 fraction of FeCPC I:Na Ol mixture and so on.

The hydrodynamic diameter (D_h) (in nm) and zeta-potential (in mV) are crucial parameters to determine the nature (size and surface charge) of the catanionic system. The size and zeta-potential value of different fractions are presented in Fig. 2. Fig. 2(a&b) shows the change in D_h and zeta-potential of 1 mM FeCPC I:Na Ol fractions and Fig. 2(c&d) shows the change in D_h and zeta-potential of 0.1 mM vesicular fractions, respectively. Table S1 lists the value of PDI at both concentrations for all fractions. These fractions behave similarly at both concentrations. Exponential growth in the hydrodynamic diameter was observed for samples with the increase in the proportion of cationic component of the metallosurfactant i.e. from V19 to V91 fraction. For instance (Fig. 2(a)), at 1 mM fraction V19 exhibits the minimum size (100 nm), whereas V91 the observed size was 700 nm. Zeta-potential of anionic rich

side carries anionic surface charge as expected: Zeta-potential value for fraction V19 to V37 showed a surface charge around -50 mV to -30 mV. All the other fractions have a positive charge of around +55 mV which is due to the more cationic content in the mixture. Similarly, D_h and zeta-potential of 0.1 mM vesicular fractions calculated, for fractions (V19 to V73) showed a size around 200 nm, however, with the increase in FeCPC I content in FeCPC I:Na Ol size increases to 500 nm and 650 nm for V82 and V91 fractions, respectively. (Fig. 2(c)). For zeta-potential first three fractions (Fig. 2(d)) V19, V28, and V37 have charges around -40 mV while all other fractions carry a positive charge. PDI for all fractions other than V82 and V91 is less than 0.5 which also indicates the monodispersity in the system (Table S1). The obtained data confirmed that with an increase in metallosurfactant content in the total fraction of FeCPC I:Na Ol there was an increase in the size of the vesicular system. In general, vesicles with zeta-potential that vary between + 30 mV to -30 mV not formed aggregates. Most of these vesicular fractions have a zeta-potential of more than +30 mV or less than -30 mV which confirms that these synthesized MCVs have excellent colloidal stability.

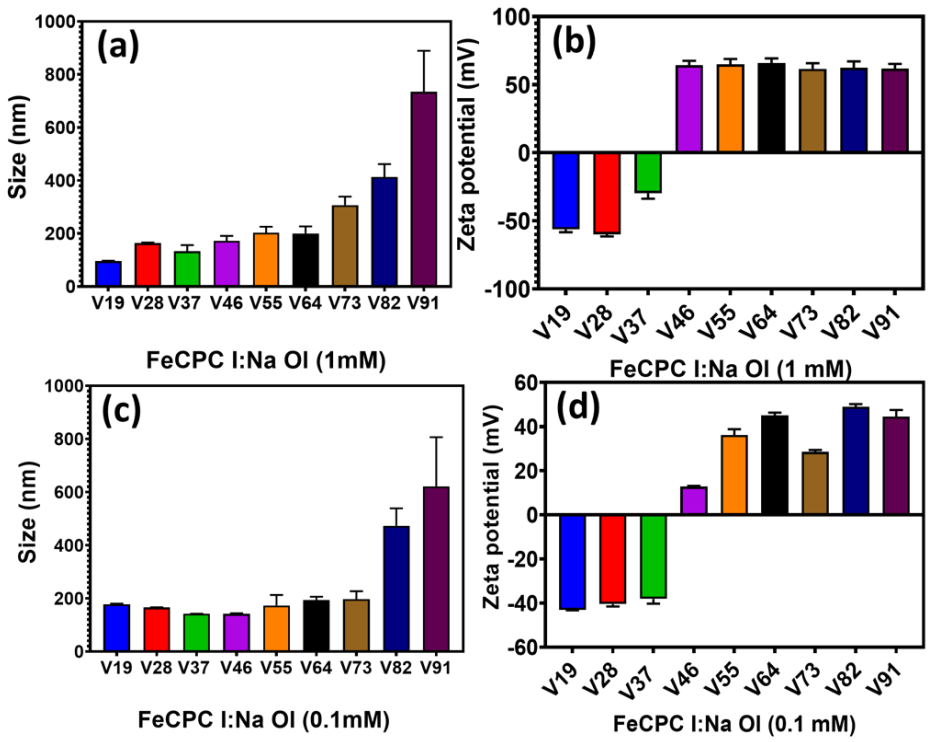

Fig. 2 DLS and Zeta-potential charactrization of synthesized FeCPC I:Na-Ol metallocatanionic vesicles fractions (a) size (nm) and **(b)** zeta-potential (mV) of FeCPC I:Na Ol (1 mM), **(c)** size (nm) and **(d)** zeta-potential (mV) of FeCPC I:Na Ol (0.1 mM).

For further studies, two fractions were selected out of all the fractions at 0.1 mM. The spontaneous and stable catanionic vesicles always require one of the surfactants in excess that gives a net charge on vesicles that also cause significant colloidal stabilities [27]. One is from the anionic rich side i.e V37 and the other is the cationic rich side i.e V73 were chosen. These fractions exist in between on both sides from FeCPC I:Na Ol equimolar ratio. Both these fractions have a size of less than 200 nm with good PDI (Table S1) The hydrodynamic diameter in PBS was monitored by DLS for one month (Table S2) at intervals, to estimate the stability of these selected V37 and V73 catanionic mixtures. Both fractions showed good stability order in solution for up to 1 month. For the V37 fraction, the vesicle's size on a freshly prepared sample was 142 nm and after a month it increases up to 253.8 nm with PDI less than 0.5 nm. In the case of V73, size and PDI almost remained close by for one month. After one week size does not seem to change in both fractions.

Cryo-TEM and FEG-SEM were employed to study the structural distribution, morphology, and integrity of the prepared vesicles on selected fractions V37 and V73. Samples for cryo-TEM were prepared at room temperature. Fig. 3 (a) and (b) show the uni-lamellar spherical structure of the V37 and V73 fractions, respectively. Fig. 3(c) and 3(d) showed the FEG-SEM images of V37 and V73 vesicular structures which further confirms the spherical morphology of the catanionic system. The size obtained from the cryo-TEM technique for V37 and V73 is smaller than the size obtained from the DLS. This is because the DLS technique gives estimated size by measuring the hydrodynamic diameter plus double liquid layer around the vesicles while cryo-TEM gives the actual estimate of particle size.

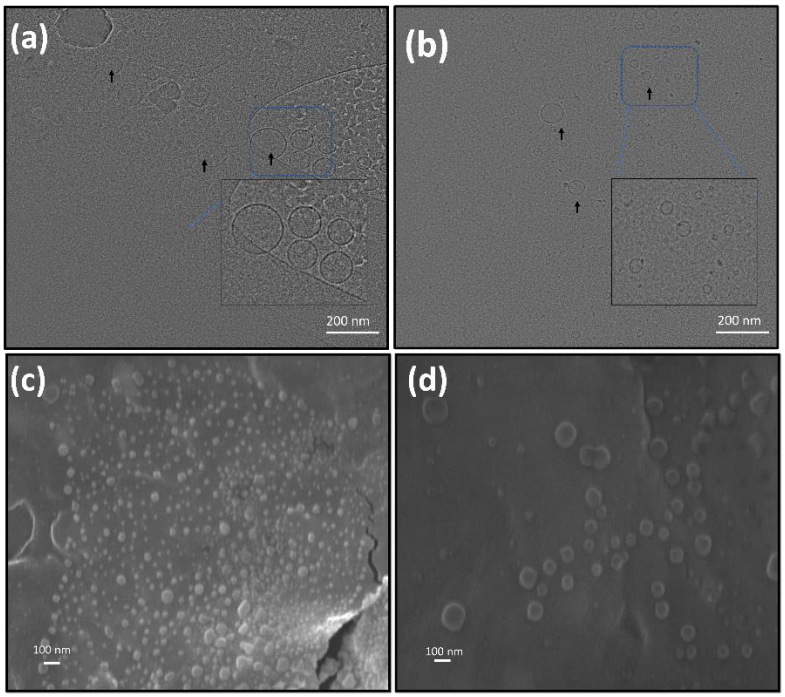

Fig. 3 MCVs morphology characterization images, Cryo-TEM images of **(a)** V37, and **(b)** V73 (size bar 200 nm); FEG-SEM images of **(c)** V37, and **(d)** V73 fractions.

Next ICP-MS analysis was performed to check the amount of Fe present in the prepared V37 and V73 fractions. We have found that in V37 amount of Fe was 117.04 µg/L and in the V73 fraction, it was 247.58 µg/L. ICP-MS study revealed that metallosurfactant rich fractions have more amount of Fe in comparison to Na Ol rich V37 fractions.

Fluorescence spectroscopy was utilized to characterize the encapsulation of MB into the vesicles. Fluorescence emission spectra of MB loaded V37 and V73 vesicles fractions were recorded and compared with the spectra of free MB to estimate the loading concentration. There was a decrease in the fluorescence intensity of MB when we mixed them with vesicular fractions (Fig. S2). By using encapsulation efficiency eq. 1 this change in PS fluorescence emission spectra was calculated and MB encapsulation was found to be 12.05 % and 20.30 % with V37 and V73 fractions, respectively, compared to free MB. This shows that the metallosurfactant rich fraction has higher encapsulation as compared to Na Ol rich (V37) fraction. Fig. S2 suggests that a higher decrease in fluorescence intensity for V73

vesicular fraction as compared to the V37 fraction. Furthermore, V37 and V73 vesicular fractions containing MB were characterized using zeta-potential measurement (Table S2). The empty vesicles V37 and V73 have zeta potential values of -38.1 mV and 28.5 mV, respectively. After loading with MB, the values fluctuated to -37 mV for V37 and +23 mV for the V73 fraction. These results suggest that cationic MB decreases the anionic surface charge of V37 fractions and the cationic surface charge of the V73 fraction and confirms successful encapsulation of MB.

Further stability of two selected MB@V37 and MB@V73 fractions were studied in acidic, neutral, and basic conditions. MB@V37 and MB@V73 fractions were prepared in 5, 7, and 9 pH solutions and hydrodynamic size and PDI values were calculated by employing DLS for two week. The measured value of size and PDI are given in Table S3. This study confirmed that prepared MB@MCVs V37 and V73 fractions are stable in this studied condition. Their size and PDI values increased with time. In addition to this, MCV V37 and V73 fractions morphology was checked after loading MB. HR-TEM and FE-SEM analysis were performed. Fig. 4(a&b) shows the HR-TEM images of MB@V37 and MB@V73 fractions, respectively. Fig. 4(c&d) shows the FE-SEM images of MB@V37 and MB@V73 fractions, respectively. Both microscopy investigations confirmed that vesicles morphology remained undisturbed after PS loading into vesicles.

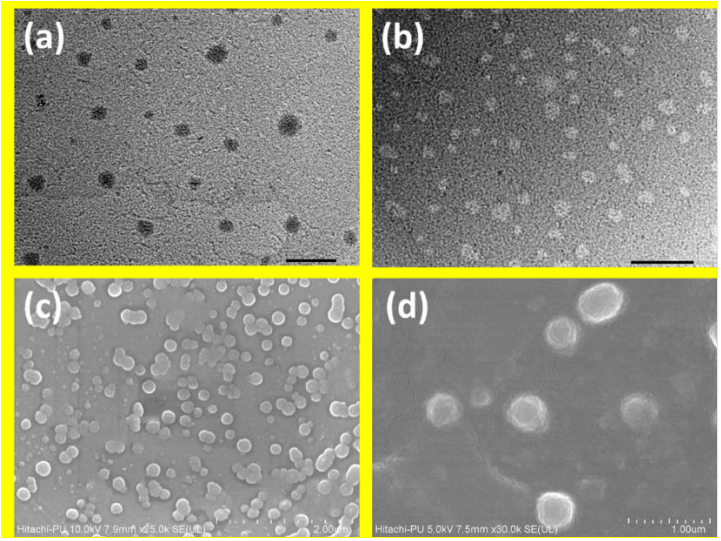

Fig. 4 MB@MCVs morphology characterization images, HR-TEM images of MB with **(a)** V37, and **(b)** V73 (size bar 1 µm); FEG-SEM images of MB with **(c)** V37, and **(d)** V73 fractions.

Also, the FEG-SEM study was carried for MB@V37 and MB@V73 fractions at the above-studied pH environment. Fig. S2(a-c) shows the FEG-SEM images of MB@V37 and MB@V73 fractions at 5, 7 and 9 pH. HR-TEM analysis was also performed on metallosurfactant rich cationic charge carried MB@V73 fraction at same pH environment. Fig. S3(a-c) shows the HR-TEM images of the MB@V73 fraction at 5, 7, and 9 Ph, respectively. This microscopic study confirmed that in this studied pH environment condition prepared MB@MCVs fractions were remained stable.

3.2. In-situ Singlet Oxygen Generation: The efficiency of MB-loaded MCVs to produce $^1O_2$ upon irradiation with red laser was evaluated using ABMA assay. ABMA is a well-known water-soluble dye that shows high sensitivity towards $^1O_2$, which can be monitored by following the quenching in fluorescence emission intensity. Upon excitation with 650 nm laser for 2 min, ABMA alone or empty V37 and V73 samples did not show any quenching in the fluorescence intensity of ABMA suggesting these samples do not generate any $^1O_2$ (Fig. 5a and S4 a-c). On the other hand, MB alone (0.5 µM) or the MCVs loaded with MB showed a significant decrease in ABMA fluorescence suggesting $^1O_2$ generation. Importantly, MB-loaded vesicles produced more $^1O_2$ generation compared to MB alone (Fig. 5a and S4 d-f). This could be due to the presence of metal ions within the catanionic vesicles, which have been shown to enhance $^1O_2$ generation by reducing the self-quenching caused by the aggregation of MB as well as by improving the photophysical properties of the MB by promoting the intersystem crossing, triplet PS^3 quantum yield and fluorescence lifetime in the excited state. Therefore, based on the obtained data, it can be concluded that these Fe-metallocatanionic vesicles enhance the efficiency of $^1O_2$ generation from MB [28,29].

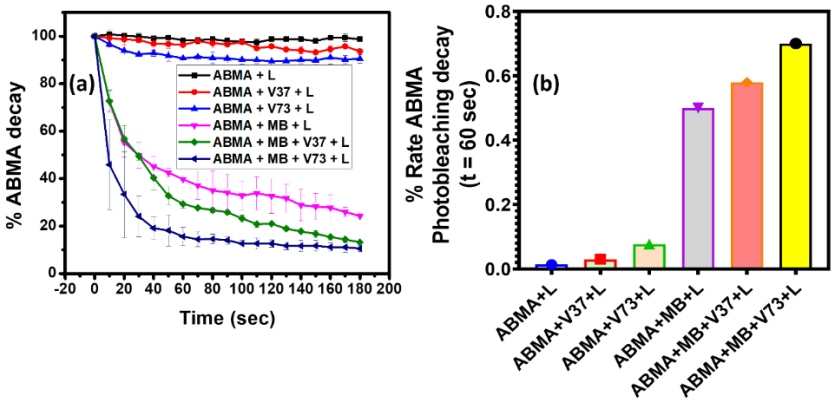

Fig. 5 Red light-mediated generation of singlet oxygen from MB-loaded Metallocatanionic vesicles. (a) Time-dependent singlet oxygen generation as a function of change in fluorescence intensity of ABMA (at 405 nm) from different MCVs. **(b)** Rate of change in ABMA photobleaching for a period of 60 sec per PS concentration.

The time-dependent changes in ABMA fluorescence intensity after irradiation in different samples are plotted in Fig. 5(a). This shows an extremely fast and high decrease in ABMA fluorescence emission intensity when MB was encapsulated to V73 as compared to V37 and pure MB. This rate of ABMA photobleaching was calculated per 60 sec and per MB (2 µM) concentration (Fig. 5(b)) by using a reported formula [30,31].

The percentage rate of ABMA photobleaching for various combinations under irradiation is given in Fig. 5(b). The results confirmed that there was no effect of laser on ABMA as the percentage rate of ABMA photobleaching was 0.01 % The value reaches 0.030 % and 0.077% with V37 and V73 fractions, respectively when empty vesicles were used, and this implies that an insignificant amount of $^1O_2$ was generated from pure vesicles. % rate of ABMA photobleaching was 0.5 % when pure MB was used under irradiation. While, it increases to 0.58% and 0.70%, for MB-loaded vesicles V37 and V73, respectively. For MB with V37 and V73 fractions, there was a 0.1-fold and 0.40-fold increase in the $^1O_2$ generation was observed, respectively These results indicate that there was an increase in $^1O_2$ efficiency

of pure MB after loading in the vesicles system and this increase was more with the V73 vesicular system as compared to V37.

3.3 In vitro studies:

3.3.1 Biocompatibility, photodynamic therapy, and cellular uptake: Encouraged by the *in-situ* $^1O_2$ generation capability of the MCVs synthesized in this work, we next evaluated the biocompatibility, photo-toxicity and cellular uptake of these MB loaded MCVs in MCF-7 cells. Firstly, the dark toxicity (no laser irradiation) of the free MB, empty and MB-loaded MCVs incubated with MCF-7 cells for 48 h was evaluated using WST-8 metabolic activity assay at various concentrations (0.5 µM to 0.75µM) (Fig. 6(a)). These empty and MB-loaded MCVs showed a negligible reduction in metabolic activity of MCF-7 cells under dark, suggesting the non-toxic nature of these MCVs even a high concentration of 0.75 µM. While comparing the toxicity of these MCVs with free MB and the untreated control group we found that there was no significant change in metabolic activity. Next, we analyzed the photodynamic effect of the MCVs (0.2 µM and 0.75 µM) incubated with MCF-7 cells by illuminating the cells with a red diode laser (650 nm and 50 mW) for 10 min. All the MB-loaded MCVs showed a concentration-dependent significant decrease in metabolic activity compared to untreated control. While MB-loaded V73 MCVs caused a 40% and 80% decrease in metabolic activity, the V37 MCVs reduced the metabolic activity of MCF-7 cells by 25% and 50% at a concentration of 0.2 and 0.75 µM, respectively (Fig. 6(b)). Interestingly, MB-loaded V73 MCVs showed higher phototoxicity compared to the V37 control. Furthermore, free MB and empty vesicle did not elicit any changes in the metabolic activity, suggesting the MCVs mediated the enhanced phototoxic effect of MB. To analyze whether the distinct susceptibility to MB-loaded vesicles was due to differences in their uptake, we analyzed the intracellular level of MB fluorescence using a fluorescence microscope (Fig. 6(c-f)). After incubation with MB-loaded MCVs, MCF-7 cells were fixed

and counterstained with DAPI (blue) and actin tracker (green) in order to evaluate the proper localization of red fluorescence of MB-loaded MCVs. Overlapping MB and actin fluorescence were observed within the cells treated with free MB or MB-loaded MCVs, suggesting their uptake within MCF-7 cells. Strong fluorescence was observed in cells incubated with V73 MCVs (Fig. 6(d)) compared to V37 MCVs or MB alone (Fig. 6(e&f). This higher uptake of V73 compared to V37 MCVs could be due to the presence of a higher cationic component which results in a zeta potential of + 23 mV versus -37 mV for V37, which causes an enhanced electrostatic interaction with MCF-7 cells (zeta potential = -20 mV) [32,33]. Furthermore, similar to previously reported literature a poor cellular uptake of MB was observed [34]. This distinct cellular uptake profile explains the obtained difference in the photo-toxicity of free MB and MB-loaded V73 & V37 MCVs. Thus, based on the obtained data it can be concluded that the MCVs are biocompatible PS delivery vehicles, which due to their catanionic nature improves the uptake of MB and enhances the efficiency of PDT due to the presence of a metal ion.

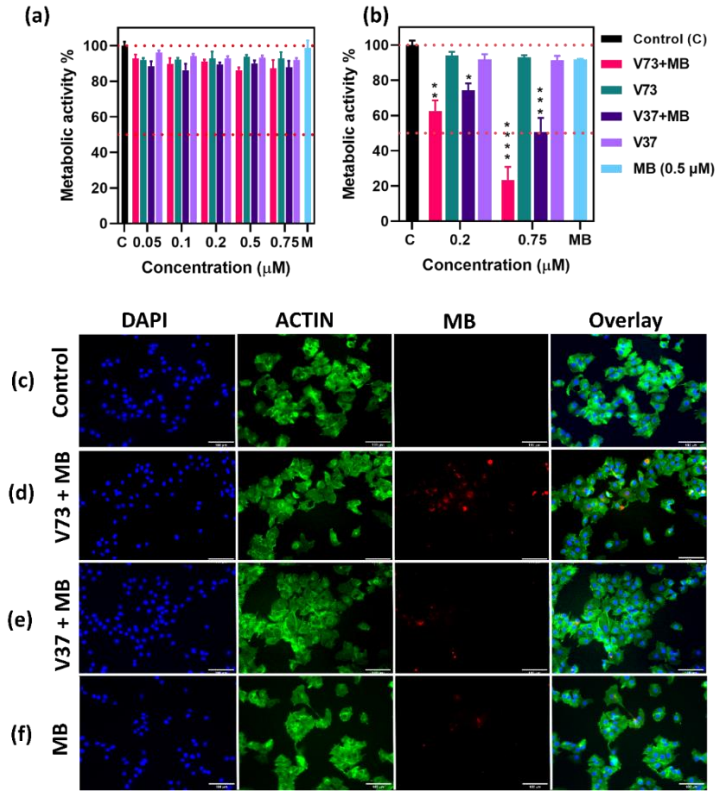

Fig. 6 In vitro cytotoxicity and uptake of MB-loaded MCVs in MCF-7 cells. (a) Dark toxicity and **(b)** photo-toxicity of MB-loaded MCVs at various concentrations were analyzed using WST-8 assay upon exposure with a red laser (650 nm, 50 mW) for 10 min. The experiment was performed using triplicates and the data are expressed as mean ± S.E.M. Statistical significance at ****$p < 0.0001$ *vs* untreated control (denoted as C) was calculated using 2-way ANOVA with Tukey post-test. **(c-f)** Cellular uptake of MB-loaded MCVs was analyzed using a fluorescence microscope. DAPI (blue) – nucleus, actin (green) – cytoskeleton and red - MB-loaded MCVs. Scale bars = 100 µm.

In literature, there was only one article available, for use of CVs in PDT. Castagnos *et al*. reported the use of lactose-derived tricatenar based CVs for chloroaluminium phthalocyanine (ClAlPc) PS delivery and applied *in vitro* PDT on melanoma cell line (B16-F10) and oral squamous cell carcinoma (OSCC) cell lines. In this article, they have not discussed the *in situ* $^1O_2$ generation ability of ClAlPc alone and after loading into CVs. However, they found an increase in *in vitro* phototoxicity against both cell lines [35]. This prepared FeCPC I:Na Ol MCVs formulation enhanced the both *in situ* $^1O_2$ generation ability of MB and also it enhanced the *in vitro* phototoxicity against MCF-7 cells.

3.3.2. Intracellular $^1O_2$ generation and cancer cell killing effect of MB loaded MCVs: To confirm intracellular $^1O_2$ generation, MCF-7 cells were incubated MB loaded MCVs before red laser irradiation and $^1O_2$ generation was detected using SOSG, which is converted to a fluorescent green derivative (endoperoxide) upon reactive with $^1O_2$, immediately after 10 min laser exposure. Strong green fluorescence was observed in all the MCVs samples, on the other hand, free MB and untreated cells showed very weak and no fluorescence, respectively (Fig. 7(a)). Both MB-loaded V73 and V37 MCVs showed a concentration-dependent increase in $^1O_2$ generation. However, V73 MCVs showed a substantial $^1O_2$ generation, this could be attributed to higher uptake of V73 fraction compared to V37 MCVs. $^1O_2$ generation was

quantified by calculating the integrated fluorescence intensity per area of the fluorescence image using ImageJ [36] (Fig. 7(b)). The obtained data indicate V73 and V37 MCVs produce significantly higher $^1O_2$ as compared to free MB, respectively. This implies that MB-loaded MCVs mediated enhancement in intracellular $^1O_2$ generation. Fig. S5 showing the overlay of dark and fluorescence images of SOSG fluorescence.

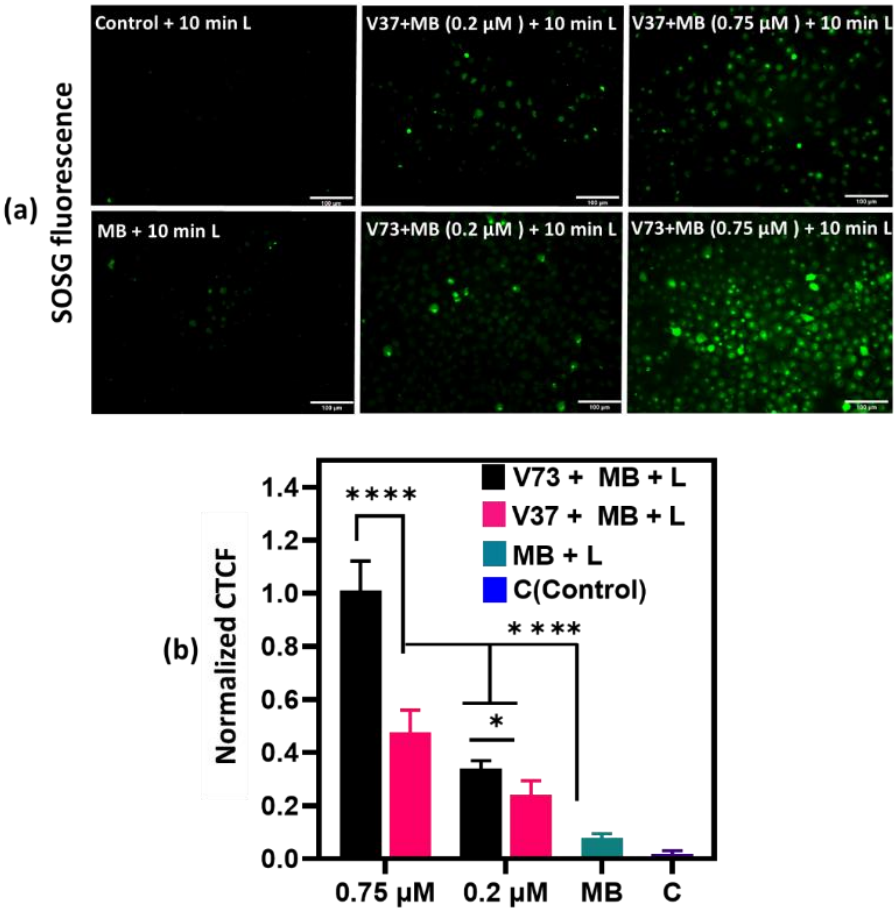

Fig. 7 Intracellular $^1O_2$ generation in MCF-7 cells treated with MB-loaded MCVs upon irradiation with 650 nm laser for 10 min. (a) Fluorescent microscopy images showing $^1O_2$ generation from different MCVs. Scale bars = 100 µm. **(b)** Integrated fluorescence intensity per area as a function of $^1O_2$ generation.

Next, to confirm $^1O_2$ mediated membrane damage and cell death, we performed DNS assay 4h after 10 min PDT. This assay is based on staining the nucleus using two different DNA

intercalating dyes viz. Hoechst 33342 and Propidium iodide (PI). Hoechst was used to stain the nucleus of all cells (dead or alive) thus represent the total number of cells, while, on the other hand, PI was used to stain the DNA of only dead cells caused by $^1O_2$ mediated membrane damage [37]. A few red spots corresponding to the fluorescence of PI were observed in cells treated with MB alone, while no fluorescence was detected in the untreated control group (Fig. 8(a&b)). The high fluorescence signal of PI was observed in cells treated with MB-loaded V37 and V73 MCVs at a concentration of 0.75 uM (Fig. 8(c&d)), suggesting MB-loaded MCVs increase cell death within 4h of PDT compared to MB alone.

Overall, these results show that Fe containing catanionic vesicles not only facilitates the uptake of MB but also enhances the efficiency of $^1O_2$ generation. Furthermore, combined with negligible dark toxicity, high photo-toxicity, deep red fluorescence of these Fe containing nano-sized colloidal vesicles a promising candidate for application in simultaneous imaging and delivery of other hydrophobic yet clinically important PSs for the PDT of deep-lying tumors.

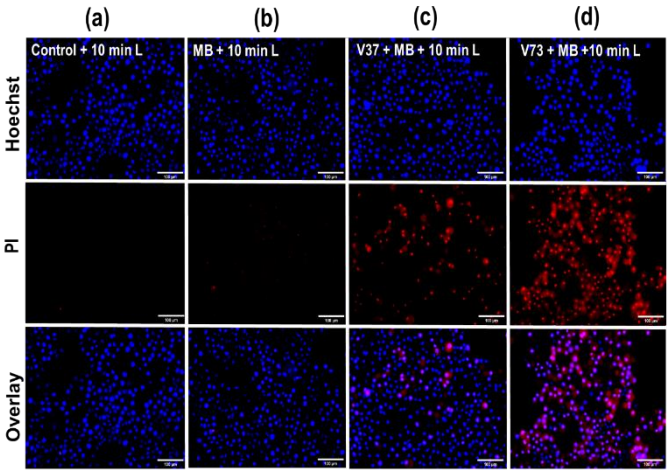

Fig. 8 Fluorescence microscopic images of live/dead MCF-7 cell line after stained with Hoechst(blue)/PI (red) after PDT in presence (a) control untreated cells, **(b)** MB, **(c)** MB-

loaded V37 and **(d)** MB-loaded V73 vesicles fraction after laser light irradiation for 10 min. Blue and Red colors represent the DNA of cells and dead cells, respectively.

4. Conclusions: In summary, we synthesized MCVs using single-chain cationic iron-metal-based metallosurfactant (FeCPC I) in combination with anionic single-chain sodium oleate (Na Ol). These synthesized MCVs with fractions 70:30 (V73) and 30:70 (V37) showed excellent colloidal stability for a period of up to a month. Cryo-TEM and FEG-SEM analysis revealed V37 and V73 fractions show unilamellar structure with a size of 100 nm. In-situ singlet oxygen study showed that the synthesized MCVs enhanced the singlet oxygen generation efficiency of MB by improving its photophysical properties. This increase was higher with metallosurfactant dominant fraction i.e V73 as compared to V37. The MCVs further enhanced the rate of ABMA photobleaching by pure MB alone when loaded in metallocatanionic vesicles suggesting the vital role of metallosurfactant in singlet oxygen enhancement of MB. Finally, these MB-loaded vesicles systems were applied for *invitro* PDT of MCF-7 human breast cancer cells. The synthesized MCVs showed negligible dark toxicity while on the other hand after irradiation with diode laser light (wavelength 650 nm, power 50 mW) for 10 min MB-loaded V73 MCVs caused a significant reduction (nearly 80%) in metabolic activity of MCF-7 cells by as compared to the V37 MCVs and free MB. Moreover, intracellular $^1O_2$ generation and different nuclear staining analyses revealed that the MB-loaded metallosurfactants based FeCPC I: Na Ol MCVs enhance singlet oxygen mediated cancer cell death within 4h after irradiation with 650 nm light. The presence of cationic and anionic charges on these vesicles increases the future research opportunities of these formulations in different drug delivery systems. Although, the PDT effects of MB-loaded MCVs in cancer treatment will need further justification through animal study.

Supporting information: Table S1. List of the PDI value calculated for all fractions at 1 mM and 0.1 mM concentration. Table S2. Metallocatanionic vesicles measured size and PDI

value of V37 and V73 fraction till 1 month. Fig. S1. Fluorescence emission spectra of free MB and MB containing vesicles. Fig. S2. Fluorescence emission spectra of ABMA after different treatments (a) only Laser (L) (b) only V73+ L (c) V37+ L (d) MB + L (e) MB + V37 + L (f) MB + V73 + L Fig. S3. Intracellular singlet oxygen generation in MCF-7 cells treated with MB-loaded MCVs upon irradiation with 650 nm laser for 10 min. Overlay images (fluorescent microscopy + Bright field) showing $^1O_2$ generation from different MCVs. Scale bars = 100 µm.

ORCID:

Bunty Sharma: 0000-0003-2495-6288

Akhil Jain: 0000-0003-2019-2030

Lluisa Perez-Garcia: 0000-0003-2031-4405

Frankie J. Rawson: 0000-0002-4872-8928

Ganga Ram Chaudhary: 0000-0003-0501-6071

Gurpreet Kaur: 0000-0002-8985-3186

Author Contributions:

Bunty Sharma and Akhil Jain have contributed equally to this work. **Experimental planning, design, and execution**: B.S,. A.J., and G.K. **Original draft:** B.S. and A.J. **Data Analysis:** B.S., A.J., and J. A. W. **Reviewing and editing:** B.S., A.J., L.P.G, F.J.R., G.R.C., and G.K. **Resources:** L.P.G., J. A. W., F.J.R., G. R. C., and G. K. **Supervision:** G.K., G.R.C., and L.P.G. **Funding:** G.K., G.R.C., L.P.G., and F.J.R.

Acknowledgment: B. Sharma wants to thank Commonwealth split-site scholarship (INCN-2019-409) and DST Inspire SRF (IF170098). G. Kaur is thankful to DST for INSPIRE

faculty award (IFA-12-CH-41). G. R. Chaudhary is thankful to UGC, India for INDO-US 21st century knowledge initiative project [F. No. 194-2/2016(IC)]. This work was supported by the European Regional Development Fund (FEDER) Spanish government grant PID2020-115663GB-C32. This work was also supported by the Engineering and Physical Sciences Research Council [Grant numbers EP/R004072/1, EP/L022494/1]. The authors would like to thank the Nanoscale and Microscale Research Centre (NMRC), the University of Nottingham for instrumentation and facility provided.

Conflicts of interest: There are no conflicts to declare.

Reference-

[1]. R. Baskaran, J. Lee, and S. G. Yang, *Biomater. Res*., 2018, **22**, 25.

[2]. J. Xiao, H Cong, S. Wang, B. Yu and Y. Shen, *Biomater. Sci*., 2021, **9**, 2384-2412.

[3]. Z. Zhou, J. Song, L. Nie, and X. Chen, *Chem. Soc. Rev*., 2016, **45**, 6597-6626.

[4]. X. Deng, Z. Shao, and Y. Zhao, *Adv. Sci*., 2021, **8**, 2002504.

[5]. S. Benson, F. de Moliner, A. Fernandez, E. Kuru, N. L. Asiimwe, J. S. Lee, L. Hamilton, D. Sieger, I. R. Bravo, A. M. Elliot, Y. Feng, and M. Vendrell, *Nat. Commun*., 2021, **12**, 2369.

[6]. L. Cheng, C. Wang, L. Feng, K. Yang, and Z. Liu, *Chem. Rev*., 2014, **114**, 10869-10939.

[7]. X. Zhao, J. Liu, J. Fan, H. Chao, and X. Peng, *Chem. Soc. Rev*., 2021, **50**, 4185-4219.

[8]. F. Akhtar, A. U. Khan, L. Misba, K. Akhtar, and A. Ali, *Eur. J. Pharm. Biopharm*., 2021, **160**, 65-76.

[9]. L. Sun, W. Jiang, H. Zhang, Y. Guo, W. Chen, Y. Jin, H. Chen, K. Du, H. Dai, J. Ji, and B. Wang, *ACS Appl. Mater. Interfaces*, 2019, **11**, 2302-2316.

[10]. J. P. Tardivo, A. D. Giglio, C. S. de Oliveira, D. S. Gabrielli, H. C. Junqueira, D. B. Tada, D. Severino, R. F. Turchiello, and M. S. Baptista, *Photodiagnosis Photodyn Ther*., 2005, **2**, 175-191.

[11]. T. Bollhorst, K. Rezwan, and M. Maas, *Chem. Soc. Rev*., 2017, **46**, 2091-2126.

[12]. M. Dubois, B. Deme, T. G. Krzywicki, J. C. Dedieu, C. Vautrin, S. Desert, E. Perez, T. Zemb, *Nature*, 2001, **411**, 672-675.

[13]. V. V. Dhawan, and M. S. Nagarsenker, *J. Control Release*, 2017, **266**, 331-345.

[14]. K. Tsuchiya, H. Nakanishi, H. Sakai, and M. Abe, *Langmuir*, 2004, **20**, 2117-2122.

[15]. J. Liu, Y. Jiang, Y. Cui, C. Xu, X. Ji, and Y. Luan, *Int. J. Pharma.*, 2014, 560-571.

[16]. N. Manghisi, C. Leggio, A. Jover, F. Meijide, N. V. Pavel, V. H. S. Tellini, J. V. Tato, R. G. Agostino, L. Galantini, *Angew. Chem. Int. Ed*., 2010, **49**, 6604-6607.

[17]. W. Li, T. Luo, Y. Yang, X. Tan, and L. Liu, *Langmuir*, 2015, **31**, 5141-5146.

[18]. P. Gong, Z. Chen, Y. Chen, W. Wang, X. Wang, and A. Hu, *Chem. Commun*., 2011, **47**, 4240-4242.

[19]. Pradeep, G. Kaur, G. R.; Chaudhary, and U. Batra, *J. Colloid Interface Sci.*, 2020, **562**, 598-607.

[20]. B. Sharma, V. Thakur, G. Kaur, and G. R. Chaudhary, *ACS Appl. Bio. Mater*., 2020, **3**, 8515-8524.

[21]. H. Mehta, G. Kaur, G. R. Chaudhary, and U. Batra, *Corros. Sci*., 2021, **179**, 109102.

[22]. P. Kaushik, G. Kaur, G. R. Chaudhary, and U. Batra, *J. Colloid Interface Sci.*, 2021, **582**, 894-905.

[23]. G. Kaur, P. Garg, B. Kaur, G. R. Chaudhary, S. Kumar, N. Dilbaghi, P. A. Hassan, and S. L. Gawali, *Soft Matter*, 2018, **14**, 5306-5318.

[24]. R. C. F. G.; Lopes, O. F. Silvestre, A. R. Faria, M. L. C. do Vale, E. F. Marques, and J. B. Nieder, *Nanoscale*, 2019, **11**, 5932-5941.

[25]. S. Geng, Y. Wang, L. Wang, T. Kouyama, T. Gotoh, S. Wada, and J. Y. Wang, *Sci. Rep*., 2017, **7**, 39202-39215.

[26]. N. A. Kuzbetsova, N. S. Gretsova, O. A. Yuzhakova, V. M. Negrimovskii, O. L. Kaliya, and E. A. Luk'yanets, *Russ. J. Gen. Chem*., 2001, **71**, 36-41.

[27]. S. A. Safran, P. Pincus, and D. Andelman, *Science*, 1990, **248**, 354.

[28]. A. Steinegger, Y. Moritz, and S. M. Borisov, *J. Photochem. Photobiol. A*, 2021, **407**, 113046-

[29]. L. B. Josefsen, and R. W. Boyle, *Met. Based Drugs*, 2008, **2008**, 276109.

[30]. O. Penon, M. J. Marin, D. A. Russell, L. Pérez-García, *J. Colloid Interface Sci.*, 2017, **496**, 100-110.

[31]. O. Penon, M. J. Marin, D. B. Amabilino, D. A. Russell, L. Pérez-García, *J. Colloid Interface Sci.*, 2016, **462**, 154-165.

[32]. Y. Zhang, M. Yang, J. H. Park, J. Singelyn, H. Ma, M. J. Sailor, E. Ruoslahti, M. Ozkan, and C. Ozkan, *Small*, 2009, **5**, 1990-1996.

[33]. O. V. Bondar, D. V. Saifullina, I. I. Shakhmaeva, I. I. Mavlvutova, and T. I. Abdullin, *Acta Naturae*, 2012, **4**, 78-81.

[34]. P. T. Wu, C. L. Lin, C. W. Lin, N. C. Chang, W. B. Tsai, and J. Yu, *Nanomaterials*, 2018, **9**, 14.

[35]. P. Castagnos, M P. Siqueira-Moura, P. L. Goto, E. Perez, S. Franceschi, I. Rico-Lattes, A. Tedesco and M. Blanzat, *RSC Adv*. 2014, **4**, 39372-39377.

[36]. A. Jain, P. G. J. Pournier, V. Mendoza-Lavaniego, P. Sengar, F. M. Guerra-Olvera, E. Iniguez, T. G. Kretzschmar, G. A. Hirata, and P. Juarez, *J. Nanobiotechnology*, 2018, **16**, 26.

[37]. M. E. Alea-Reyes, O. Penon, P. G. Calavia, M. J. Marin, D. A. Russell, L. Perez-Garcia, *J. Colloid Interface Sci.*, 2018, **521**, 81-90

Graphical abstract:

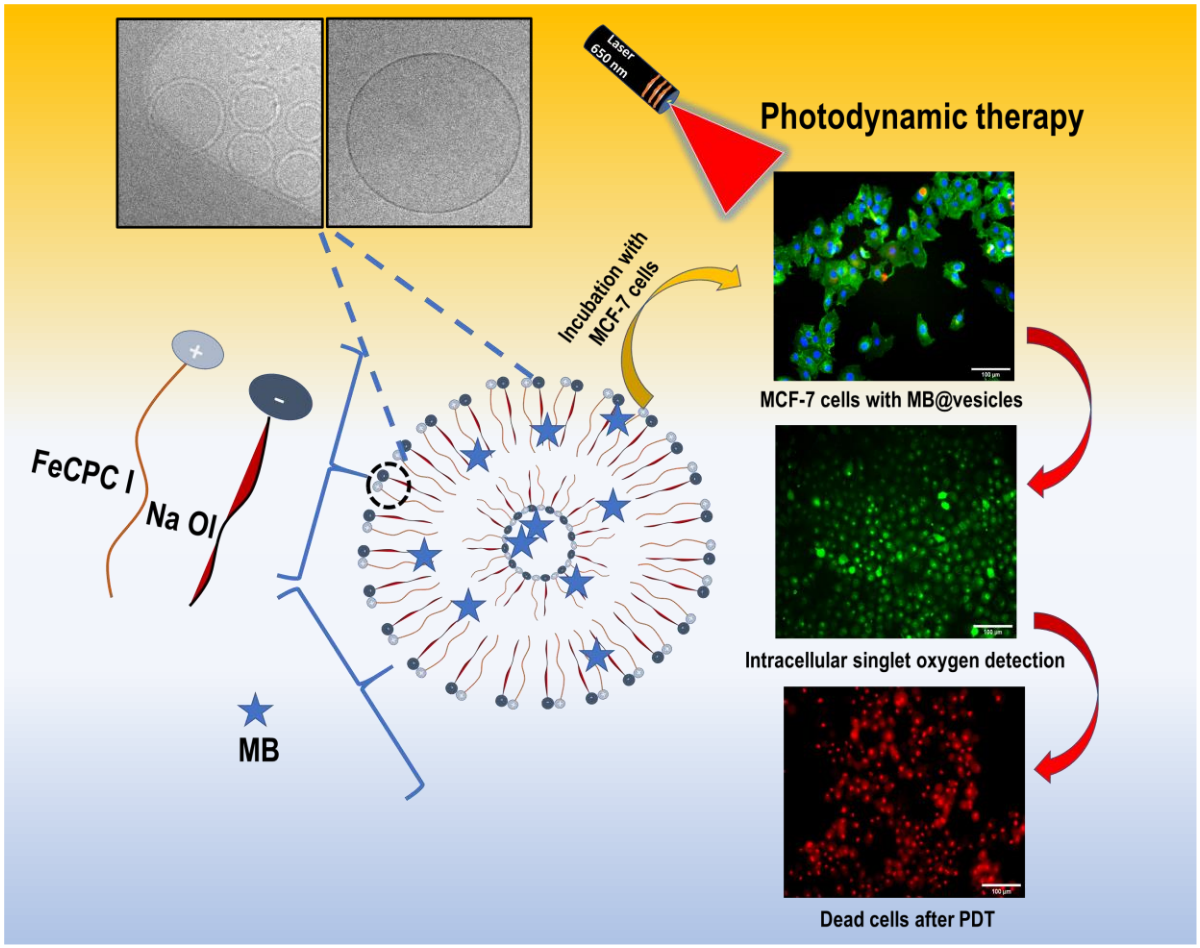
Laser
650 nm
Photodynamic therapy
Incubation with
MCF-7 cells
MCF-7 cells with MB@vesicles
FeCPC I
Na OI
MB
Intracellular singlet oxygen detection
Dead cells after PDT